processes

MDPI

Article

Formation Characterization and Type Prediction Based on Geophysical Well Log Data in Horizontal Well: A Case Study of Triassic Chang 8 Formation in Shunning Region, Central Ordos Basin

Jiaqi Li [1], Liang Xiao [1,2,*], Hui Xi [3], Ruiqiang Chi [3], Hucheng Wen [4] and Wenjing Zhang [3]

[1] School of Geophysics and Information Technology, China University of Geosciences, Beijing 100083, China; lijq0403@163.com
[2] State Key Laboratory of Geological Processes and Mineral Resources, China University of Geosciences, Beijing 100083, China
[3] Research Institute of Exploration & Development, PetroChina Changqing Oilfield, Xi'an 710018, China
[4] Engineering Supervision Department, PetroChina Changqing Oilfield, Xi'an 710018, China
* Correspondence: xiaoliang@cugb.edu.cn

Abstract: The role of the horizontal well in developing unconventional oil and gas reservoirs is particularly significant. Different from vertical wells, horizontal wells are greatly affected by many factors, e.g., well track, surrounding mudstone, resistivity, and pore structure heterogeneity in horizontal and vertical directions. These make it difficult to evaluate reservoir parameters and determine optimized test layers. In order to improve formation evaluation in horizontal wells, it is necessary to carry out the research of analyzing formation anisotropy, predict physical property parameters, and classify formation to determine high-quality intervals. In this study, taking Triassic Chang 8 Formation in Shunning Region, Central Ordos Basin as an example, 40 core samples were drilled and applied for nuclear magnetic resonance (NMR), mercury injection capillary pressure (MICP), and resistivity experiments. The porosity, permeability, resistivity, and pore structure anisotropy are analyzed. Results illustrate that the physical properties and pore structure in horizontal direction are superior to vertical direction. Meanwhile, NMR log loses its role in pore structure characterization in horizontal wells. Afterward, methods of correcting interval transit time (DT) and resistivity anisotropy are raised, and models of predicting formation physical property parameters, such as porosity, permeability, and water saturation, are established. A parameter, named as the formation type indicator (*FTI*), is proposed to reflect reservoir oil-bearing properties and pore structure. Finally, our target horizontal intervals are classified into four types, and the highest-quality "sweet spot" is determined.

Keywords: anisotropy analysis; pore structure; formation physical properties; formation classification

Citation: Li, J.; Xiao, L.; Xi, H.; Chi, R.; Wen, H.; Zhang, W. Formation Characterization and Type Prediction Based on Geophysical Well Log Data in Horizontal Well: A Case Study of Triassic Chang 8 Formation in Shunning Region, Central Ordos Basin. *Processes* **2023**, *11*, 2297. https://doi.org/10.3390/pr11082297

Academic Editor: Qingbang Meng

Received: 26 June 2023
Revised: 27 July 2023
Accepted: 30 July 2023
Published: 31 July 2023

1. Introduction

A drilling horizontal well is considered the primary method to explore unconventional oil and gas resources and increase hydrocarbon production. Compared with the vertical well, the horizontal well can traverse thousands of meters of intended intervals. Hence, it can reduce production costs and significantly improve oil and gas production [1]. The horizontal well technique has become an essential method for efficiently developing low permeability oil and gas reservoirs in the Ordos Basin [2]. In recent years, techniques and methods that focused on horizontal well log interpretation and formation evaluation were rare; models that were raised in the vertical well were still used [3]. However, log responses in horizontal intervals are absolutely different from that in vertical intervals due to the complex drilling and logging environment, intricate geometric relationship between wellbore trajectory and formation, and comprehensive influence of reservoir anisotropy. In addition, the logging series in the horizontal well is slowly updated, and

the conventional well log data are limited. As a result, formation evaluation is limited [4]. Plenty of production practices illustrate that horizontal well-staged fracturing technique can significantly increase oil drainage area, thus improving individual well deliverability by more than three times [5]. To improve the fracturing effect, horizontal intervals should be first characterized in fine detail, and classification criteria should be established to determine the best dessert belt.

Research that focuses on anisotropy evaluation of the horizontal well has garnered much interest. Many methods and techniques have been proposed [6–8]. These detailed that the induction or lateral resistivity was affected by well deviation in a uniform infinitely thick anisotropic formation, and the relationship between apparent resistivity and anisotropy coefficient was raised to correct the measured resistivity in highly deviated and horizontal wells. Klein (1993) observed that electrical anisotropy mainly occurred in thin interlayers or layered formations once formation thickness was smaller than the longitudinal resolution of resistivity tool [7]. Gao and Xie (2000) provided a rapid correction method for lateral resistivity in highly deviated well through 3D orthorectified numerical simulations [8]. All these methods were raised based on resistivity simulation, and they were not established based on measured resistivity data. As a result, the field applicability decreased. In addition, many methods were proposed to correct the interval transit time (DT) curve based on statistical regression [9,10]. These methods were available in specific regions or formations and cannot be widely used in any type of formation. Current methods can be divided into two categories for horizontal interval classification prediction. The first type of classification method was established based on the clustering technique. He et al. (2013), Wei et al. (2013), and Li et al. (2017) chose several parameters that were associated with hydrocarbon production, such as the absolute open flow, effective reservoir length, decrease in casing pressure, and casing pressure drop rate, as input and used cluster analysis method to establish horizontal well-classification evaluation criteria [11–13]. The second type of method was combined with several parameters that were associated with formation properties (porosity, permeability, oil saturation, shaly content, etc.) and hydrocarbon production (e.g., gas logging, casting sheet, and mercury injection capillary pressure (MICP) experimental data) to synthesize a comprehensive evaluation index to classify horizontal intervals [14–16]. These methods have been well-used in particular fields and achieved good results. However, some shortcomings could not be solved. First, too many production parameters were used, making it valuable only in mature development areas. Second, formation parameter calculations in the horizontal well faces great challenges before the anisotropy is first corrected. This will decrease the wide applicability. In our target Triassic Chang 8 Formation of Shunning Region, insufficient production data can be acquired, and formation physical properties prediction models are not established. These mean that current horizontal well classification methods cannot be directly used. In addition, deep research illustrates that local structures and sediments significantly control over hydrocarbon accumulation [17], manifested by differences in pore structure at the microscopic level. Therefore, complicated pore structure is a crucial factor that controls the quality of Chang 8 Member [18]. Pore structure should be considered in establishing formation classification criteria.

The purpose of this study is to propose a method to classify Triassic Chang 8 Formation in horizontal intervals and determine the "sweet spot". This method is established by combining pore structure with formation physical property parameters, such as the oil saturation and porosity. Meanwhile, models of predicting physical parameters, e.g., porosity, permeability, and water saturation, are established after formation anisotropy is first analyzed. Field examples illustrate that the proposed methods are available, and the predicted "sweet spot" area matches well with the drill stem test (DST) data.

2. Geological Setting

Ordos Basin is the second-largest sedimentary basin in China. It used to be a part of the Greater North China continental sedimentary basin [19]. However, it was separated

and transformed into a large inland basin in the late Triassic [20]. The Ordos Basin is characterized by a large asymmetric syncline with a gentle eastern flank and a steep western flank [21]. The Zhijing–Ansai oilfield is located in the west and central part of the Yinshan slope. It contains six regions, which are Jingbian in the north, Yongning in the south, Ansai in the east, Wuqi in the west, and Zhidan and Shunning in the central sections. It covers about 1.0×10^4 km^2 [22] (Figure 1). The Shunning Region is a part of the Zhijing–Ansai oilfield. It is located in the Yinshan slope structural belt and belonged to delta front deposition, close to Chang 7 high-quality source rock. It is a typical forming pattern of "upper generation and lower storage" [23,24]. Triassic Chang 8 Formation is the main oil-production zone, and formation depth ranges from 1500 to 2100 m. It is subdivided into Chang 8_1 and Chang 8_2 Formation. The formation is tight and has little natural productivity. Drilling horizontal well in the Chang 8_1 Formation is the main route that increases hydrocarbon production.

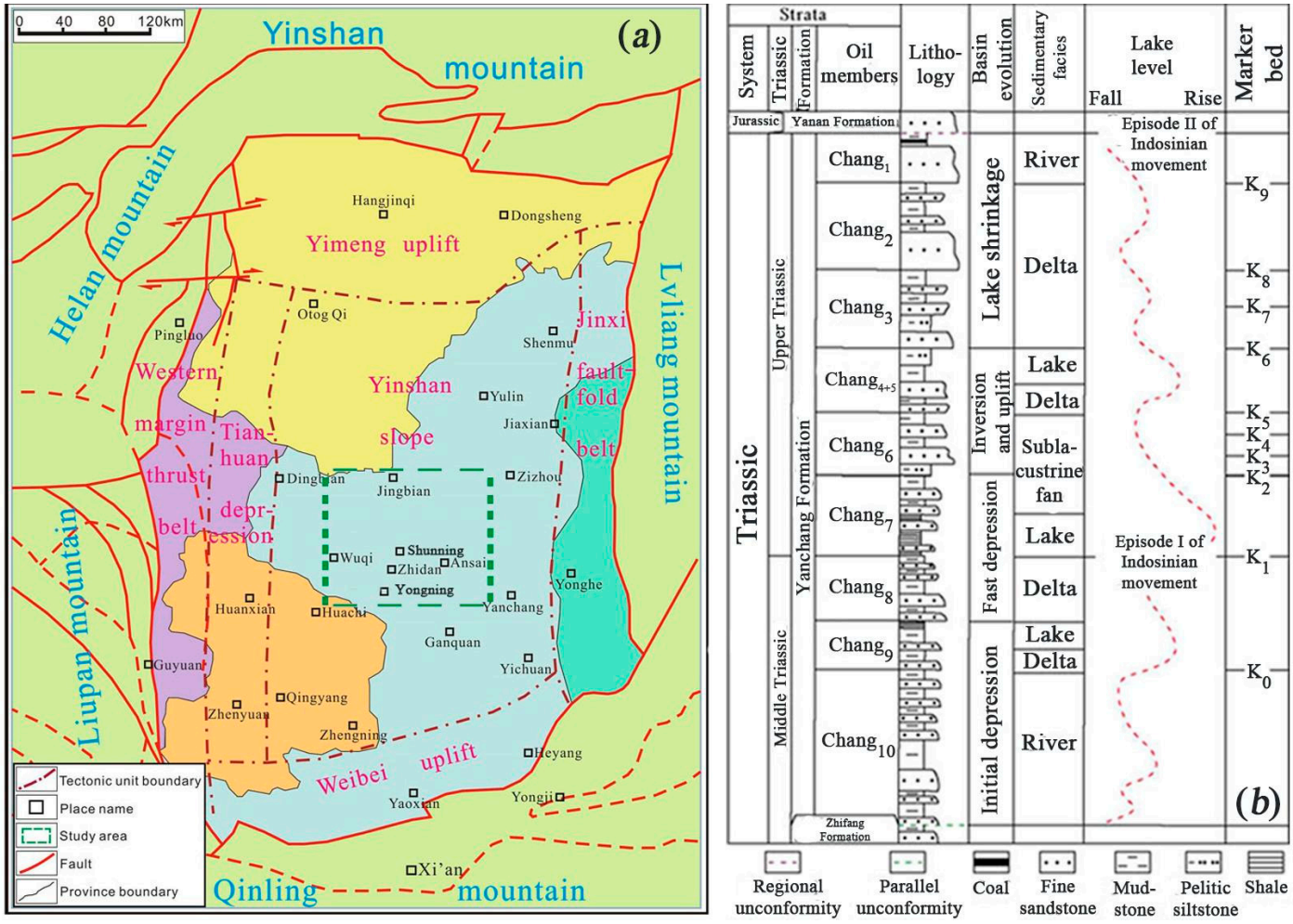

Figure 1. Location map of our target Shunning Region in Central Ordos Basin (**a**); and the formation member, thickness and lithology (**b**) [23].

3. Reservoir Characteristics of Triassic Chang 8 Formation

3.1. Lithologic Features

Based on the experimental data of the thin section that are acquired from 145 core samples, the lithology is mainly feldspar sandstone and lithic feldspar sandstone; the total content of quartz and felspar reaches to 68.88% (Figure 2a). The Chang 8 sandstones, which are close to the Chang 7 source rock, have a high content of feldspar and lithic dissolution and grain collapse from the acidic fluid injection. This also indirectly leads to the deterioration of reservoir physical properties [25]. The detrital composition is mainly metamorphic rocks and igneous rock (Figure 2b), and the interstitial matter is mainly composed of ferrocalcite and chlorite (Figure 2c).

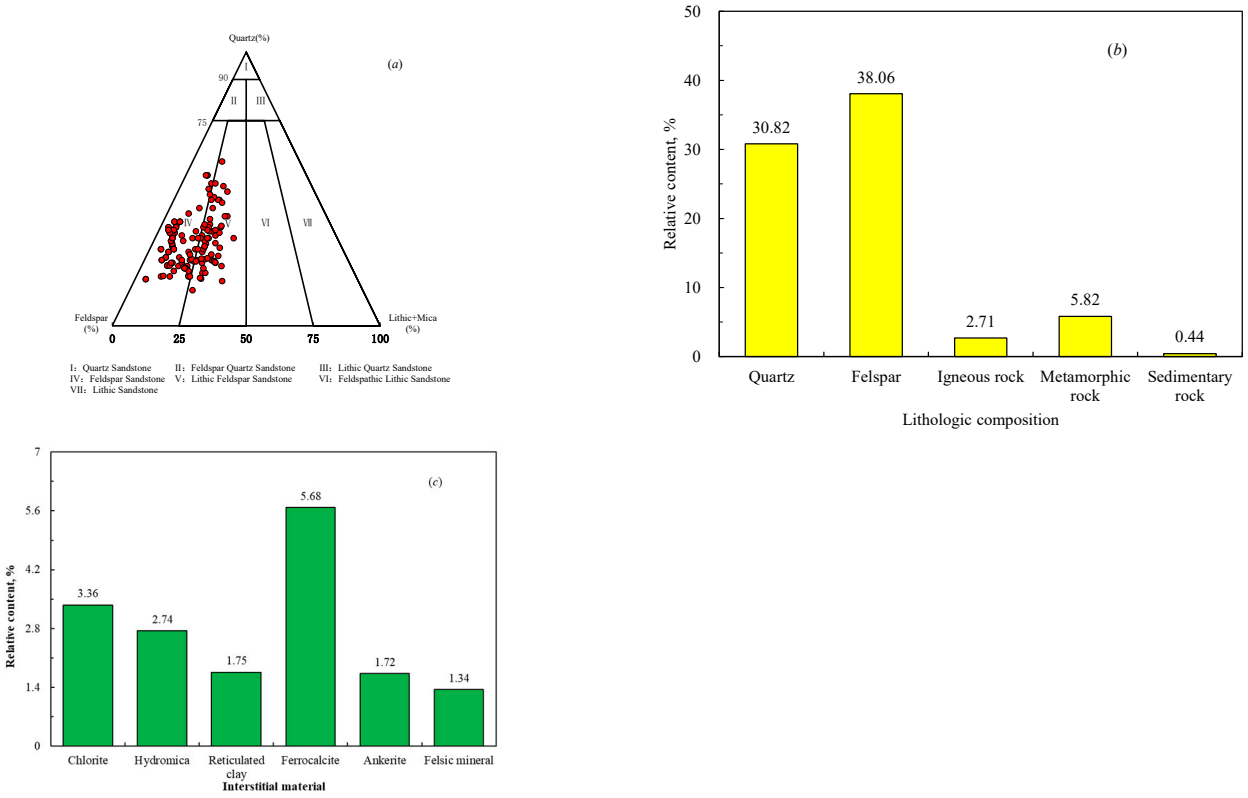

Figure 2. Lithology features (**a**) Lithologic composition; (**b**) and interstitial material (**c**) of Triassic Chang 8 Formation in Shunning Region, Central Ordos Basin.

3.2. Physical Characteristics

In Chang 8 Formation of the Shunning Region, 1988 core samples were recovered from 33 straight boreholes and applied for routine physical properties measurements. Figure 3a,b show the statistical histogram of core-derived porosity and permeability, separately. These figures illustrate that the porosities range from 4% to 12%, and the average porosity is 7.42% (Figure 3a). Permeabilities are predominantly distributed from 0.01 mD to 2 mD, and the average permeability is only 0.062 mD (Figure 3b). The relationship between the porosity and permeability is poor (Figure 3c). Figure 3a–c indicate that our target Chang 8 Member belongs to typical tight sandstone reservoirs and contains strong heterogeneity.

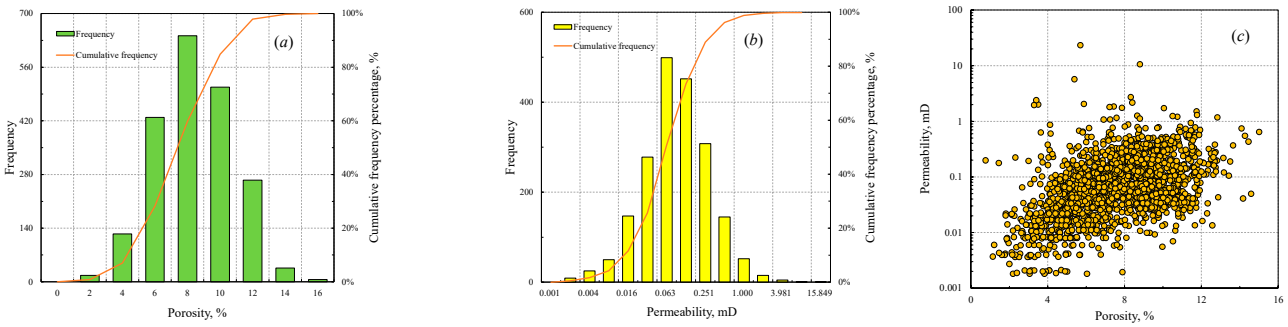

Figure 3. Histograms of core-derived porosity (**a**) Permeability; (**b**) and relationship between core-derived porosity and permeability for 1988 core samples (**c**) in the Triassic Chang 8 Member of Shunning Region in Central Ordos Basin.

3.3. Anisotropy Characteristics

In Chang 8 Formation, we drilled 40 samples along a 90-degree angle to separately obtain 20 horizontal and 20 vertical core samples, following with the method displayed in Figure 4. These core samples were applied for nuclear magnetic resonance (NMR), mercury injection capillary pressure (MICP), and resistivity experimental measurements in the laboratory, respectively.

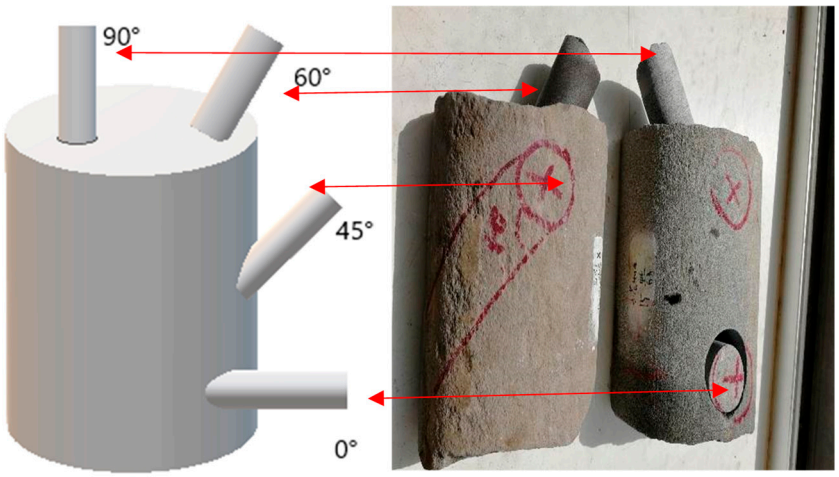

Figure 4. Principle and method of drilling core samples at any angle.

3.3.1. The Pore Structure Anisotropy

The NMR Response

Figure 5a,b exhibit the experimented NMR T_2 distribution for 20 core samples separately. T_2 spectra displayed in Figure 5a are acquired from core samples that were drilled from the horizontal direction, whereas Figure 5b shows the NMR T_2 spectra that were acquired from vertical core samples. A comparison of these two figures illustrates that the shapes of NMR T_2 distributions are similar. Irreducible water saturation (S_{wi}) and T_2 logarithmic mean (T_{2lm}) that extracted from experimented NMR data for the horizontal and vertical core samples also exhibit approximate values (Figure 6). These mean that NMR T_2 distributions are invalid in indicating formation anisotropy.

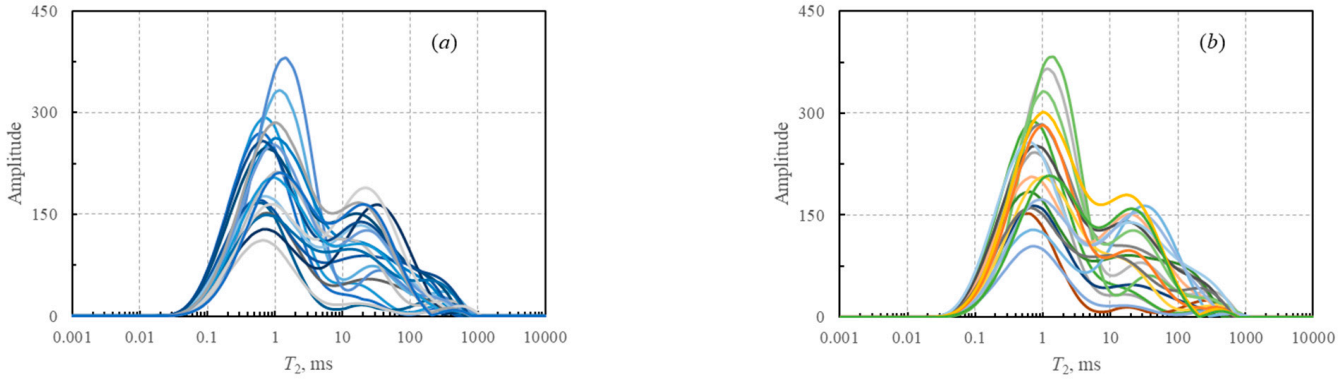

Figure 5. Comparisons of the shapes of experimented NMR T_2 distributions for 20 horizontal core samples (**a**) and 20 vertical core samples (**b**). The NMR T_2 distributions contain similar shapes, even if they were drilled from different directions. This means that NMR T_2 spectra cannot be used to indicate rock anisotropy in Chang 8 Formation.

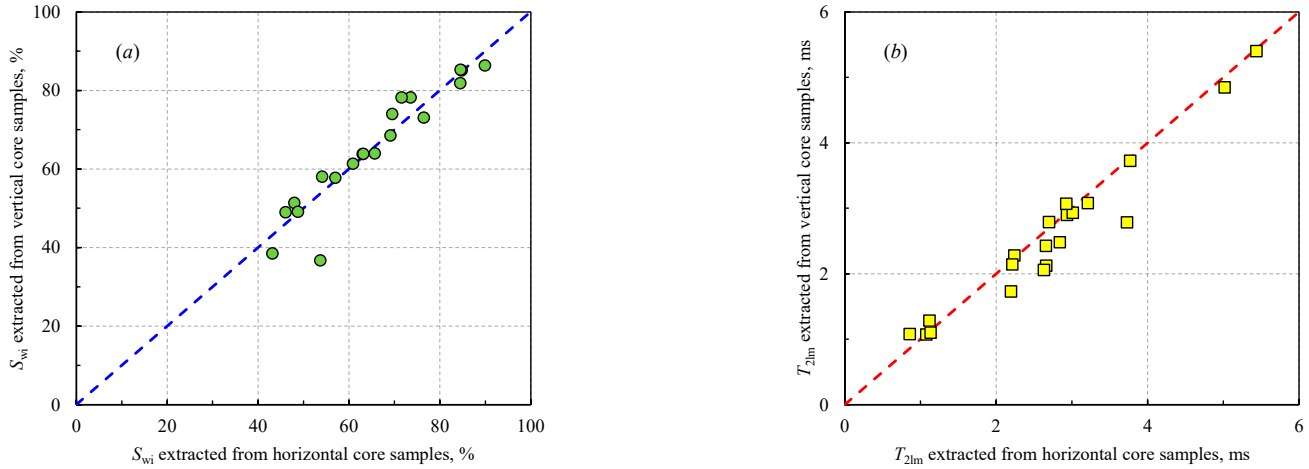

Figure 6. Comparisons of experimental S_{wi} (**a**) and T_{2lm} (**b**) for 20 horizontal and vertical core samples. These two figures illustrate that NMR experimental parameters that extracted from two types of core samples are approximate.

The failure of NMR T_2 distribution in reflecting the reservoir anisotropy can be explained as follows: for core samples with full water saturation, the NMR T_2 transverse relaxation time is dominated by surface relaxation, while the bulk relaxation and diffusion relaxation can be ignored [26]. Surface relaxation reflects the energy exchange between hydrogen nuclei and pore surfaces. Rocks with big pores always need a long relaxation time, and vice versa. The energy exchange process is independent of the angle and direction but only affected by pore size (Figure 7) [27].

The MICP Curve

We compare the shapes of MICP curves for two sets of core samples that are extracted from horizontal and vertical core samples separately (Figure 8). The location of MICP curves that are extracted from horizontal core samples is on the bottom, and the corresponding threshold pressures are low. This means that the pore structure in the horizontal direction is greater than that in the vertical direction. In Figure 9, we compare the pore structure characterization parameters (the average pore-throat radius R_m and median pore-throat radius R50) that are extracted from two different directions. A similar conclusion can be obtained. Through Figures 5–9, we can conclude that the pore structure anisotropy is strong in our target Chang 8 Formation in Shunning Region. The NMR log loses its role in pore

structure characterization in the horizontal well, whereas with the capillary pressure, the pore-throat radius distribution will be of great importance.

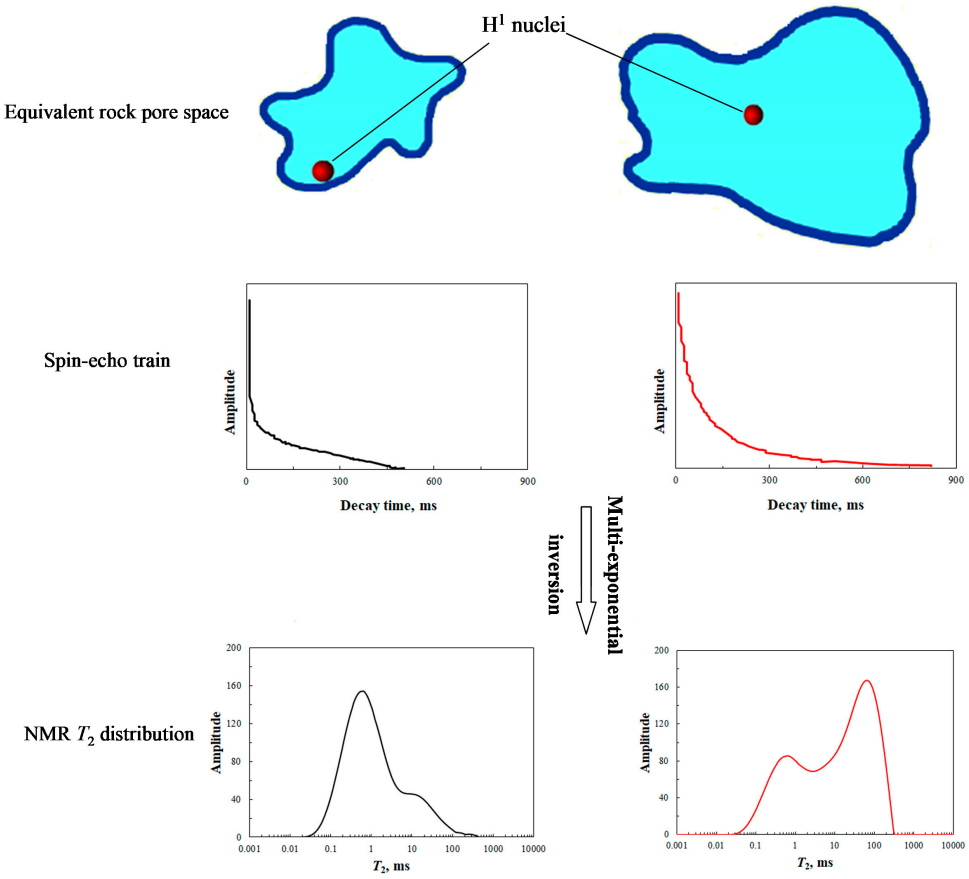

Figure 7. Relationship between rock pore size and NMR T_2 distribution.

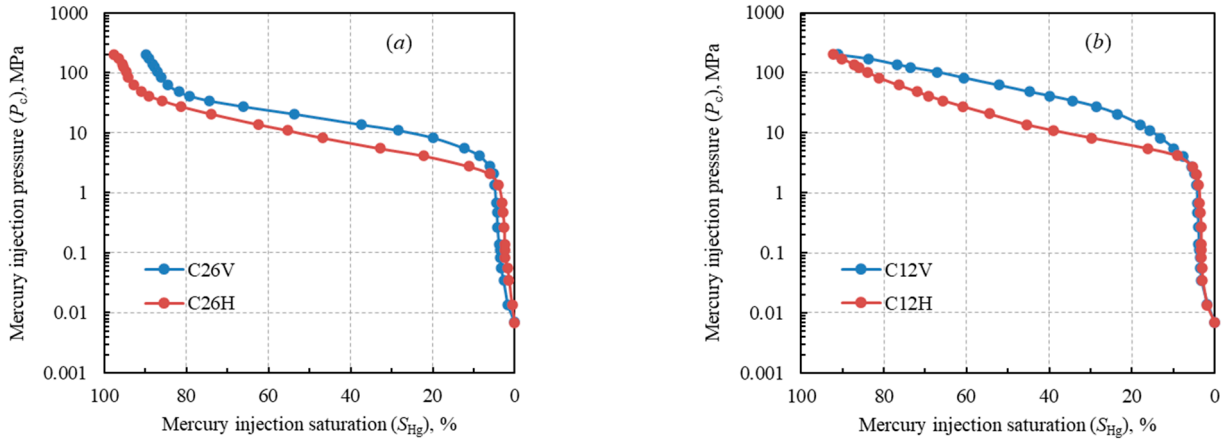

Figure 8. Comparison of horizontal and vertical MICP curves of core sample No. 26 (**a**) and No. 12 (**b**) in Chang 8 Formation in Shunning Region.

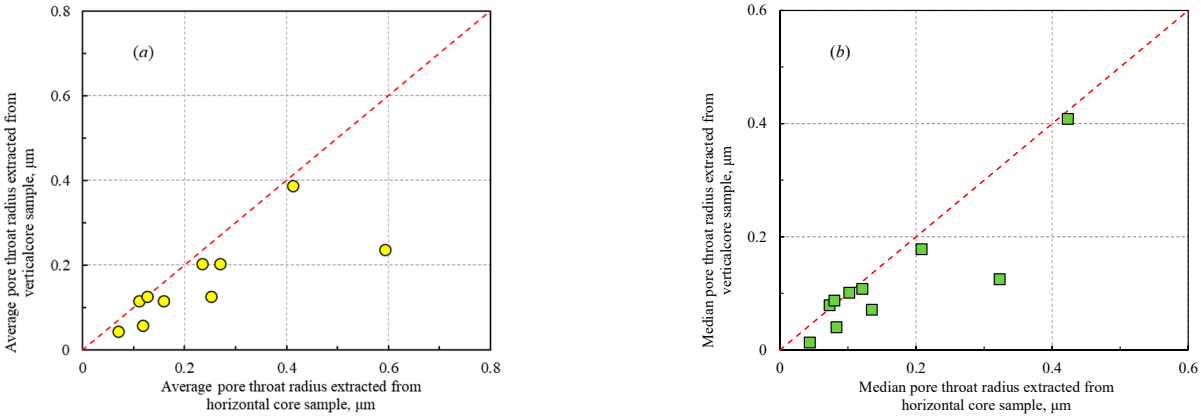

Figure 9. Comparisons of experimental the average pore-throat radius (**a**) and median pore-throat radius (**b**) for 20 horizontal and vertical core samples. These two figures illustrate that the pore structure characterization parameters extracted from horizontal core samples are superior to those in vertical direction.

3.3.2. Resistivity Anisotropy

Forty core samples are applied for resistivity experiments by a gas-drive method in the laboratory. Rock resistivities under full water and different oil saturation are acquired. The cementation exponent and saturation exponent are obtained by using cross-plots of porosity and formation factor as well as water saturation versus resistivity index, separately. In Figure 10, we compare rock resistivity under full water saturation that is measured from horizontal and vertical core samples. It can be observed that the resistivities of horizontal core samples are lower than that of vertical core samples. This is caused by the better pore structure of vertical core samples. Except for rock resistivity, the cementation exponent m and saturation exponent n are also heavily affected by formation anisotropy (Figure 11a,b). Figure 11 indicates that the values of m and n are obviously lower in the horizontal direction than in the vertical direction. This coincided with the pore structure heterogeneity. Based on the negative correlation between pore structure and rock electrical conductivity, the pore structure of horizontal core sample is superior to vertical core samples, and the corresponding values of m and n should be lower [28].

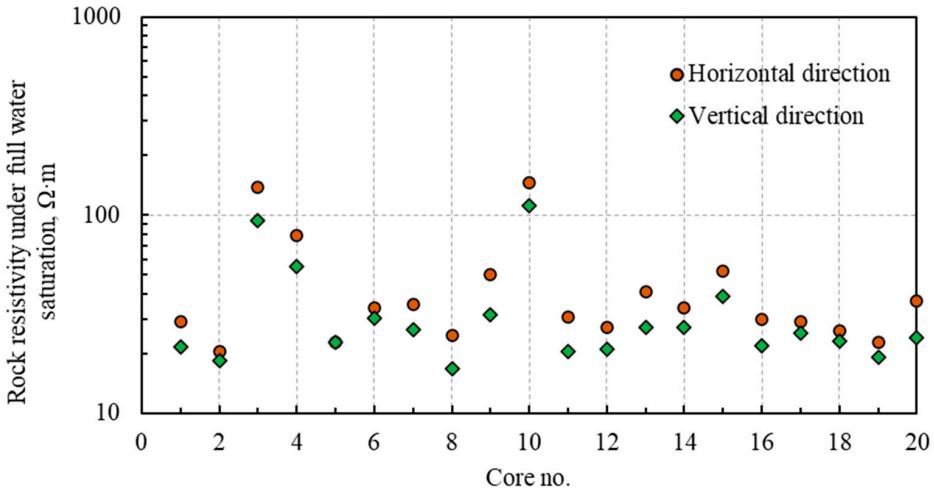

Figure 10. Comparison of experimented rock resistivities in horizontal and vertical directions under full water saturation. The pore structure in horizontal direction is better than that in vertical direction, and this leads to the decrease of resistivity in horizontal direction.

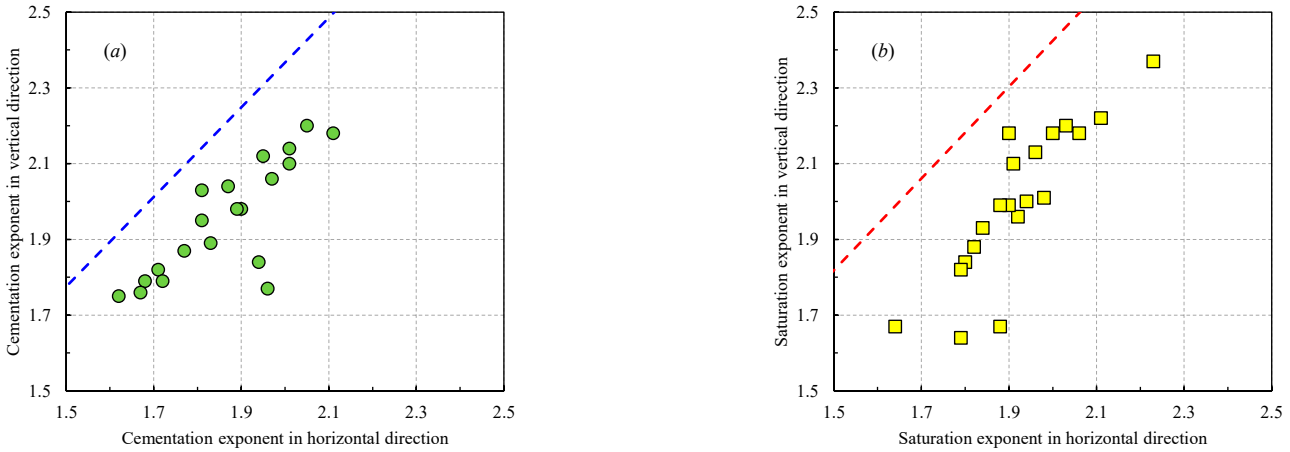

Figure 11. Comparisons of experimented cementation exponent m (**a**) and saturation exponent n (**b**) in horizontal and vertical directions for 20 core samples. m and n in horizontal direction are obviously lower than that in vertical direction due to good pore structure.

4. Methods and Models for Horizontal Well Characterization

4.1. Anisotropy Correction in Horizontal Well

Above experimental results and theoretical analysis have illustrated that the log responses of horizontal well are absolutely different from that of the vertical well in the same layer due to formation anisotropy. This leads to the established models in vertical intervals, which cannot be directly used in horizontal intervals. To predict precise formation parameters in horizontal intervals, the measured conventional log curves should be first corrected. In our target region, the measured conventional log curves contain natural gamma (GR), spontaneous potential (SP), caliper (CAL), interval travel time (DT), and deep and shallow lateral resistivity (RLLD and RLLS). Density and neutron logs are not acquired. GR, SP, and CAL have a negligible effect by the direction. However, DT, RT, and RXO are heavily affected. In this study, we correct DT and RT before they are used in horizontal interval characterization.

4.1.1. Anisotropy Correction of Interval Travel Time (DT or Δt)

In our target formation, no core samples are applied for acoustic experiments in laboratory, and the number of key wells is fewer. These means traditional interval travel time heterogeneity correction methods based on statistical regression cannot be used [9,10]. In this study, we raise a method to correct the effect of formation anisotropy to Δt, and this method covers several procedures.

First, selecting several vertical wells that are located around the target horizontal wells as control wells, collecting the Δt data of Chang 8 Formation, making a statistical histogram, collecting Δt value that represents the Chang 8 Formation based on the highest frequency, and naming it as Δt_h (Figure 12a).

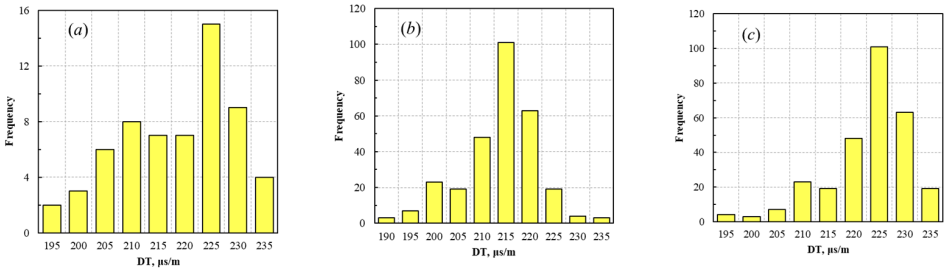

Figure 12. Statistical histograms of measured *DT* in vertical wells (**a**) In adjacent horizontal wells (**b**) and corrected DT for heterogeneity (**c**). Good consistency between (**a**,**c**) indicates that the anisotropy correction is valuable.

Second, collecting Δt data of horizontal wells in Chang 8 Formation, making a statistical histogram, recording the Δt value that corresponds to the highest frequency, and defining it as Δt_v (Figure 12b).

Third, calculating the correlation value of Δt_v and Δt_h by using Equation (1).

$$\Delta t_d = \Delta t_h - \Delta t_v \quad (1)$$

where Δt_d is the correlation value of interval travel time between horizontal and vertical directions, separately. Δt_h is the interval travel time that is acquired from horizontal direction. Δt_v is the interval travel time that is acquired from vertical direction. The unit of them is μs/m.

Combined with Figure 12a,b, the value of Δt_d is determined as +10.0 μs/m.

Finally, correcting the interval travel time of horizontal wells by adding Δt_d to the Δt curve (habitually marked as DT) and making a statistical histogram of corrected interval travel time (Figure 12c). The correction procedures will stop once the shapes of the statistical histograms of interval travel time before and after the correction are similar.

4.1.2. Anisotropy Correction of Deep Lateral Resistivity

In this study, after the formation is assumed to be composed of a bedded sequence of parallel and discrete sandstone and shale (or thin beds), and sandstone anisotropy is considered small enough to be negligible, a method is raised to correct the anisotropy of deep lateral resistivity (RLLD). This correction method covers several procedures.

First, calculating sandstone volume content (V_{ss}) and shale volume content (V_{sh}) based on GR curve by using Equations (2)–(4).

$$SH = \frac{GR - GR_{min}}{GR_{max} - GR_{min}} \quad (2)$$

$$V_{sh} = \frac{2^{GCUR \times SH} - 1}{2^{GCUR} - 1} \quad (3)$$

$$V_{ss} = 1 - V_{sh} - \varphi \quad (4)$$

where GR is the measured gamma ray in the horizontal well, GR_{min} is the gamma ray of clean sandstone, and GR_{max} is the gamma ray of pure shale; the unit of them is API. SH is the relative shale content, V_{sh} is the shale volume content, and V_{ss} is the sandstone volume content; the unit of them is v/v. φ is the porosity of the horizontal well in v/v. GCUR is a constant that is associated with the geologic period, and its value is 3.7.

Second, assigning an initial value of the horizontal resistivity of shale as R_{shho}, and calculating formation anisotropy coefficient by using Equation (5).

$$\lambda = \sqrt{(V_{ss}R_{ss} + V_{sh}R_{shho})\left(\frac{V_{ss}}{R_{ss}} + \frac{V_{sh}}{R_{shho}}\right)} \quad (5)$$

where λ is the formation anisotropy coefficient. R_{ss} is the sandstone resistivity in Ω·m. R_{shho} is the initial value of shale horizontal resistivity in Ω·m.

Third, substituting measured apparent resistivity R_a, borehole deviation angle α, and anisotropy coefficient into Equation (6) to calculate horizontal resistivity R_h:

$$R_h = \frac{R_a}{\lambda}\sqrt{(\sin^2\alpha + \lambda^2\cos^2\alpha)} \quad (6)$$

where R_h is the corrected horizontal resistivity and R_a is the measured apparent resistivity in the horizontal well; the unit of them is Ω·m. α is the borehole deviation angle in (°).

Fourth, calculating vertical resistivity R_v and horizontal resistivity of shale R_{shh} by using Equations (7) and (8).

$$R_v = \lambda^2 R_h \tag{7}$$

$$R_{shh} = \frac{V_{sh}}{\left(\frac{1}{R_h} - \frac{V_{ss}}{R_{ss}}\right)} \tag{8}$$

where R_v is the vertical resistivity with anisotropy correction, R_{shh} is the shale resistivity in horizontal direction, and the unit of them is Ω·m.

Finally, the difference between R_{shh} and R_{shho} is compared to determine if the heterogeneity correction is finished. Once the difference between R_{shh} and R_{shho} meets the accuracy requirement (lower than 0.01 Ω·m), anisotropy correction is finished and the values of R_h and R_v are considered as true formation resistivity in horizontal and vertical directions.

Based on continuous iterative calculation, the optimal values of R_{ss} and R_{shh} are defined as 110 Ω·m and 25 Ω·m, separately. By using the above-mentioned method, horizontal wells in the Shunning Region are processed, and the corrected R_h and R_v are consecutively determined. Figure 13 displays a comparison of corrected R_h and R_v with measured apparent deep lateral resistivity (RLLD). It can be observed that RLLD is absolutely different from R_h and R_v. R_h is lower than RLLD and R_v, which coincides with the experimental resistivity and can be explained by pore structure.

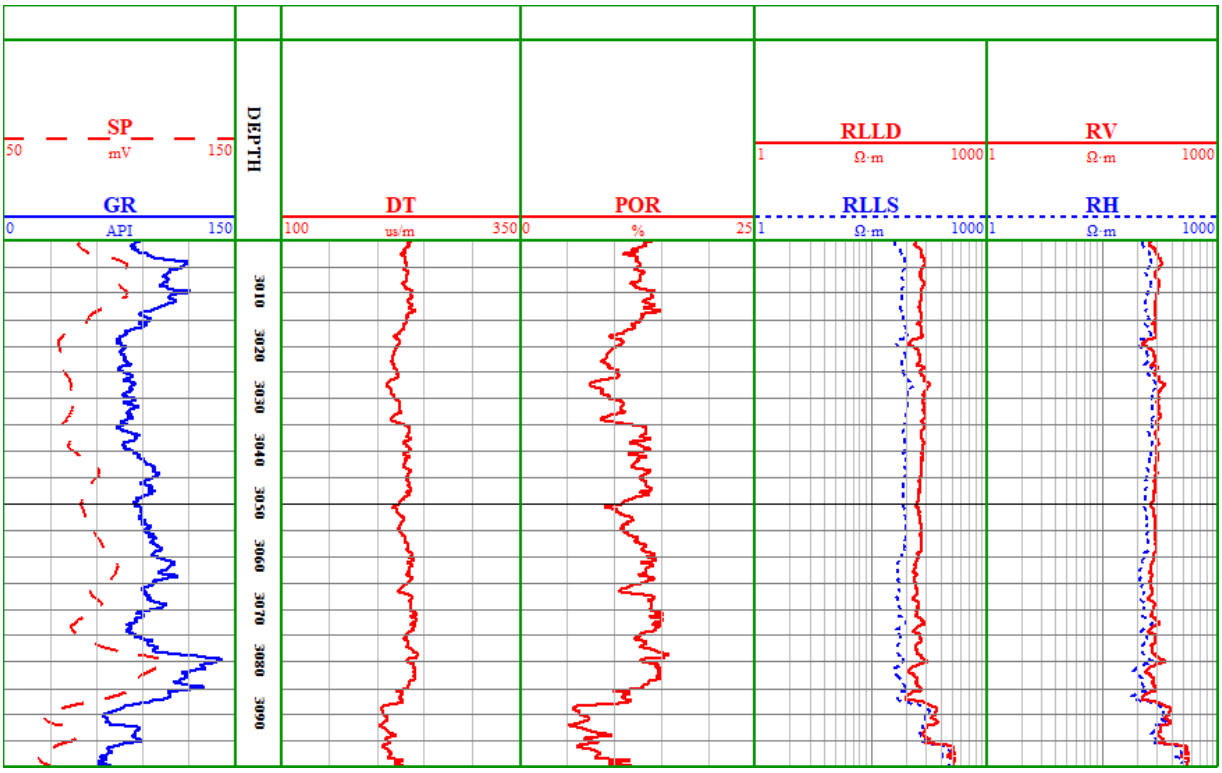

Figure 13. Resistivity anisotropy correction based on dual lateral logging in a horizontal well.

4.2. Calculation of Reservoir Physical Property Parameters

4.2.1. Porosity Calculation

We establish the porosity estimation model based on DT data because DEN and CNL are not acquired in the Chang 8 Formation. In the adjacent vertical wells, 19 core samples were recovered for routine experimental measurement. Core-derived porosity and permeability are extracted. After analyzing the core-derived and log data, we find that

Raymer's equation is optimal in expressing the relationship between core-derived porosity and DT (Figure 14). Hence, porosity estimation model is established as follows [29]:

$$\varphi = (1 - (\frac{\Delta t_c}{\Delta t_{ma}})^x) \times 100 \quad (9)$$

where φ is the porosity in %. Δt_c is the interval transit time with anisotropy correction in μs/m. Δt_{ma} is the interval transit time of rock matrix in μs/m. Generally, its value is 182 μs/m. x is the undetermined coefficient. Its value needs to be calibrated by using the experimented data of core samples. In Chang 8 Formation of Shunning Region, its value is −0.612.

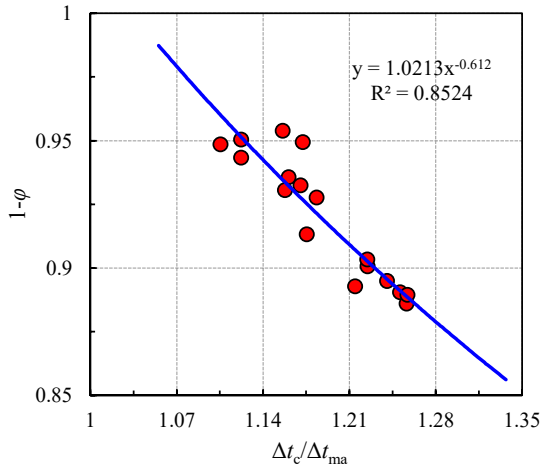

Figure 14. Model of calculating formation porosity from interval transit time based on Raymer's equation.

4.2.2. Permeability Prediction

Considering the poor relationship between core-derived porosity and permeability (Figure 3c), common permeability prediction method based on porosity cannot be used. Generally, permeability is heavily associated with the pore structure, and many models of calculating the permeability based on pore structure had been raised [30–32]. These models were proposed based on the MICP experimented data of core samples, such as the Swanson-based model, the $R10$ (pore-throat radius that corresponds to 10% mercury injection saturation)-based model, and the R_{max} (maximal pore-throat radius)-based model [30,31]. These models are verified to be effective in tight sandstone reservoirs in Ordos Basin [32]. In this study, we analyze the MICP experimental results of 20 core samples that were drilled from horizontal direction and find that permeability is heavily associated with porosity and $R10$. Hence, a permeability prediction model based on $R10$ is raised and displayed in Figure 15. The model of calculating permeability from $R10$ and porosity is expressed as Equation (10).

$$\sqrt{\frac{K}{\varphi}} = 0.197 \times R10 + 0.063 \quad (10)$$

where K is the permeability in horizontal direction in mD; φ is the porosity in horizontal direction in %; $R10$ is the pore-throat radius that corresponds to 10.0% mercury injection saturation in μm.

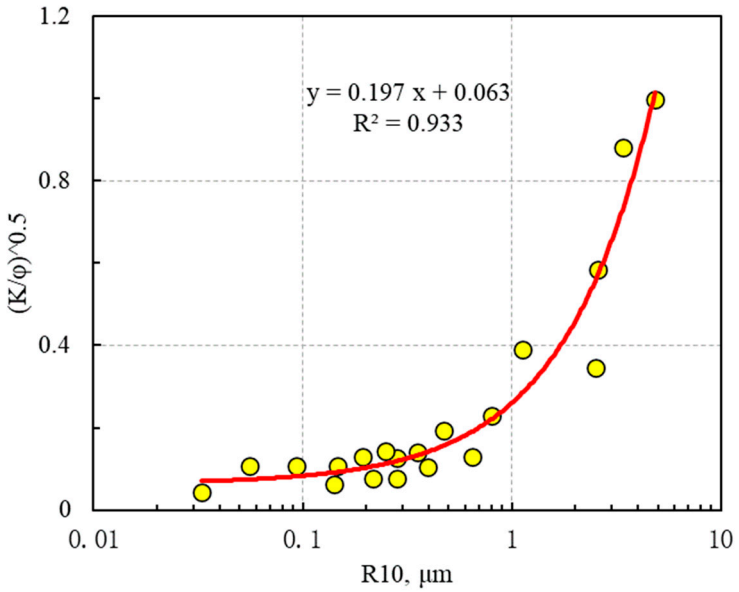

Figure 15. Relationship between core-derived porosity, permeability, and *R*10.

4.2.3. Water Saturation Calculation

Water saturation calculation models are abundant after the Archie's equation was first raised in 1942 [33]. These models contain the Simandoux equation, the Indonesian equation, the Waxman–Smits model, the dual-water model, etc. [34–39]. These models are all raised to solve the water saturation calculation in shaly sands. However, no specific models have been proposed in tight sandstone reservoirs, and the Archie's equation is still used. The derivative Archie's equation is expressed:

$$S_w = \sqrt[n]{\frac{a \times b \times R_{\mathrm{w}}}{\varphi^m \times R_{\mathrm{t}}}} \tag{11}$$

where R_{w} is the resistivity of formation water in Ω·m; R_{t} is the resistivity of rock under hydrocarbon saturation in Ω·m; S_{w} is the water saturation in v/v; a is the pore tortuosity factor; m is the cementation exponent; b is a constant that associated with lithology; and n is the saturation exponent. a, b, m, and n are defined as the rock-resistivity parameters, and their values are determined by the resistivity experiments of rocks.

In the Chang 8 Formation of the Shunning Region, we have chosen a total of 12 core samples (six from the horizontal direction and six from the vertical direction) to apply for resistivity experiments in laboratory. The relationships between porosity and formation factor, and water saturation versus resistivity index, are established in horizontal and vertical directions and displayed in Figures 16 and 17 separately. Comparing these two figures, some regularity can be concluded: (1) The resistivity properties in horizontal and vertical directions are absolutely different; this diversity can be observed by the difference of the values of a, b, m, and n. The values of m and n in the horizontal direction are lower than that of in vertical direction. (2) The relationships between water saturation versus resistivity index are all perfect. This means that the pore structure slightly affects the saturation exponent, and they can be well-used in water saturation calculation (Figures 16b and 17b). (3) Although the correlation coefficients between porosity and formation factor are high, the regressed trendline cannot well express the relation, especially for the part with porosity lower than 8% (Figures 16a and 17a). This can be demonstrated by the fact that the trend line does not cross the boundary point (1, 1). This regularity is similar to that extracted from tight gas sands in the Xujiahe Formation in the Central Sichuan Basin [28].

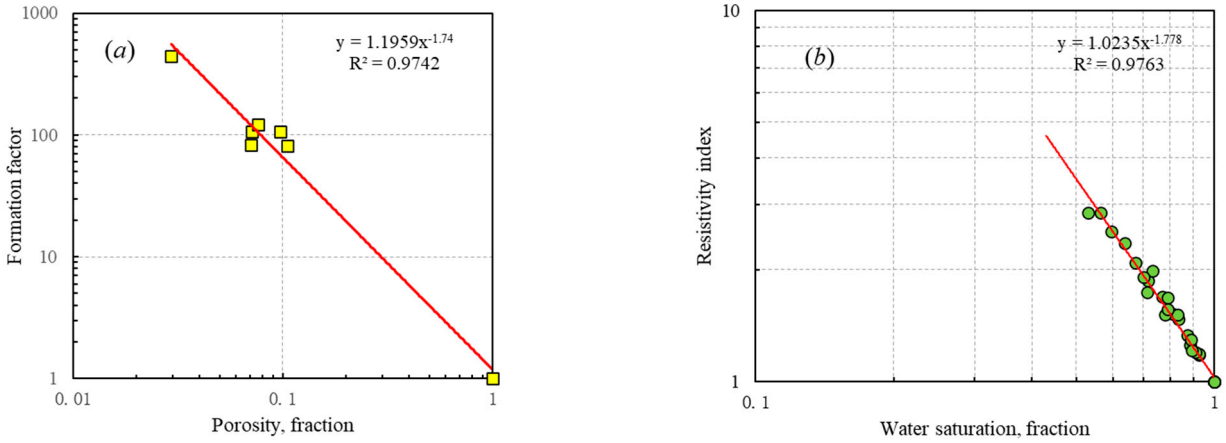

Figure 16. Cross-plots of porosity and formation factor (**a**) Water saturation versus resistivity index (**b**) for 6 core samples that were drilled from horizontal direction in Chang 8 Member of Shunning Region.

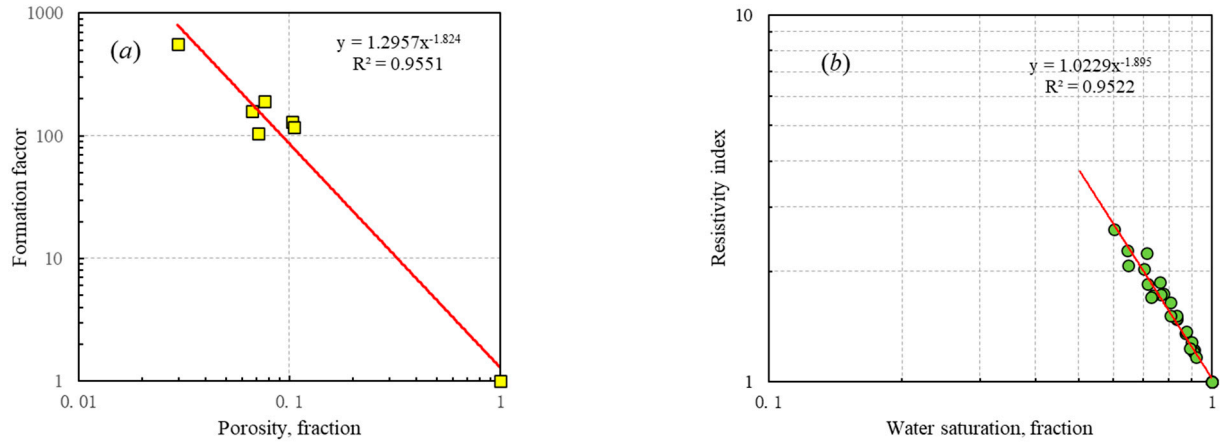

Figure 17. Cross-plots of porosity and formation factor (**a**) Water saturation versus resistivity index (**b**) for 6 core samples that were drilled from vertical direction in Chang 8 Member of Shunning Region.

To improve the accuracy of the water saturation calculation by using the Archie's equation, the cementation exponent should be optimized. Based on the theoretical analysis, Xiao et al. (2013) concluded a relation between porosity and the cementation exponent [28]. This theoretical relation can be well-used to express the variation between pore structure and cementation exponent, especially for tight rocks with porosities lower than 8%. The theoretical relation raised by Xiao et al. (2013) has been verified to be widely usable in different types of tight reservoirs [40]. In this study, using the resistivity experimental data that are displayed in Figures 16 and 17, we also analyze the effect of pore structure to cementation exponent in Chang 8 Formation of Shunning Region and determine that the cementation exponent is heavily affected by porosity. The cementation exponent decreases significantly with the increase of porosity. Based on this analysis, we optimize the relationships between porosity and formation factor and deduce two formulae to calculate various cementation exponents from porosity in horizontal and vertical directions separately (Figure 18a,b). These formulae can be expressed by Equations (12) and (13).

$$\text{Horizontal direction: } m = 0.35 \times \log(\varphi) + 2.23 \quad (12)$$

$$\text{Vertical direction: } m = 0.52 \times \log(\varphi) + 2.54 \quad (13)$$

where m is the cementation exponent; φ is porosity in v/v.

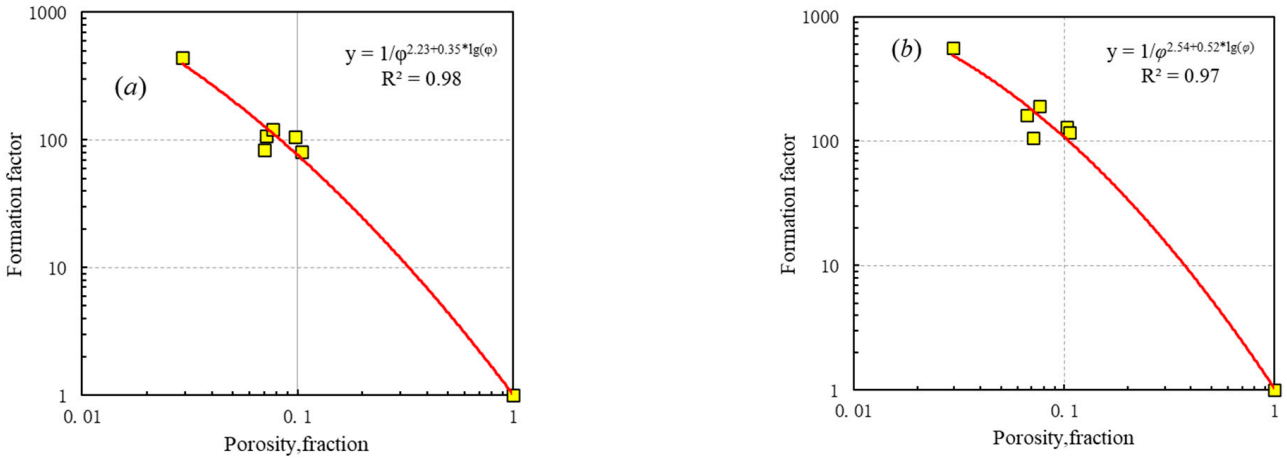

Figure 18. Optimized relationships between porosity and formation factor in tight sandstone reservoirs in horizontal (**a**) and vertical (**b**) directions in Triassic Chang 8 Formation of Shunning Region.

It should be noted that the value of a is defined as 1 in optimized relationships. Comparing Figures 16 and 17 with Figure 18, it can be easily observed that the trend lines between porosity and formation factor are deflexed once the porosities of core samples decrease. The optimized cementation exponent can well express this bendability. However, unreliable water saturation should be calculated if we directly define fixed cementation exponent in the Archie's equation.

Combining Equation (11) and Figure 16 to Figure 18, we separately conclude optimal water saturation calculation models in horizontal and vertical directions based on the Archie's equation, and these two models are expressed as:

$$S_{W\_h} = \sqrt[1.78]{\frac{1.02 \times R_w}{\varphi^{2.23+0.35*\log(\varphi)} \times R_h}} \quad (14)$$

$$S_{W\_v} = \sqrt[1.90]{\frac{1.02 \times R_w}{\varphi^{2.54+0.52*\log(\varphi)} \times R_v}} \quad (15)$$

where S_{w_h} and S_{w_v} are the calculated water saturation in horizontal and vertical directions, separately. The unit of them is v/v.

By substituting the anisotropy corrected resistivity R_h and R_v, porosity into Equations (14) and (15), S_{w_h} and S_{w_v} can be calculated. To verify the reliability of resistivity correction in the horizontal well, we also directly use the measured apparent deep lateral resistivity to calculate water saturation (S_w). Comparison of calculated S_{w_h} and S_{w_v} with S_w in a horizontal well is displayed in Figure 19. It can be observed that S_{w_h} and S_{w_v} are almost equal, whereas the value of S_w is about 5% to 8% higher. This means that the resistivity anisotropy correction is essential before it is applied for formation evaluation, or else the hydrocarbon volume will be underestimated. Either S_{w_h} or S_{w_v} can represent true formation water saturation.

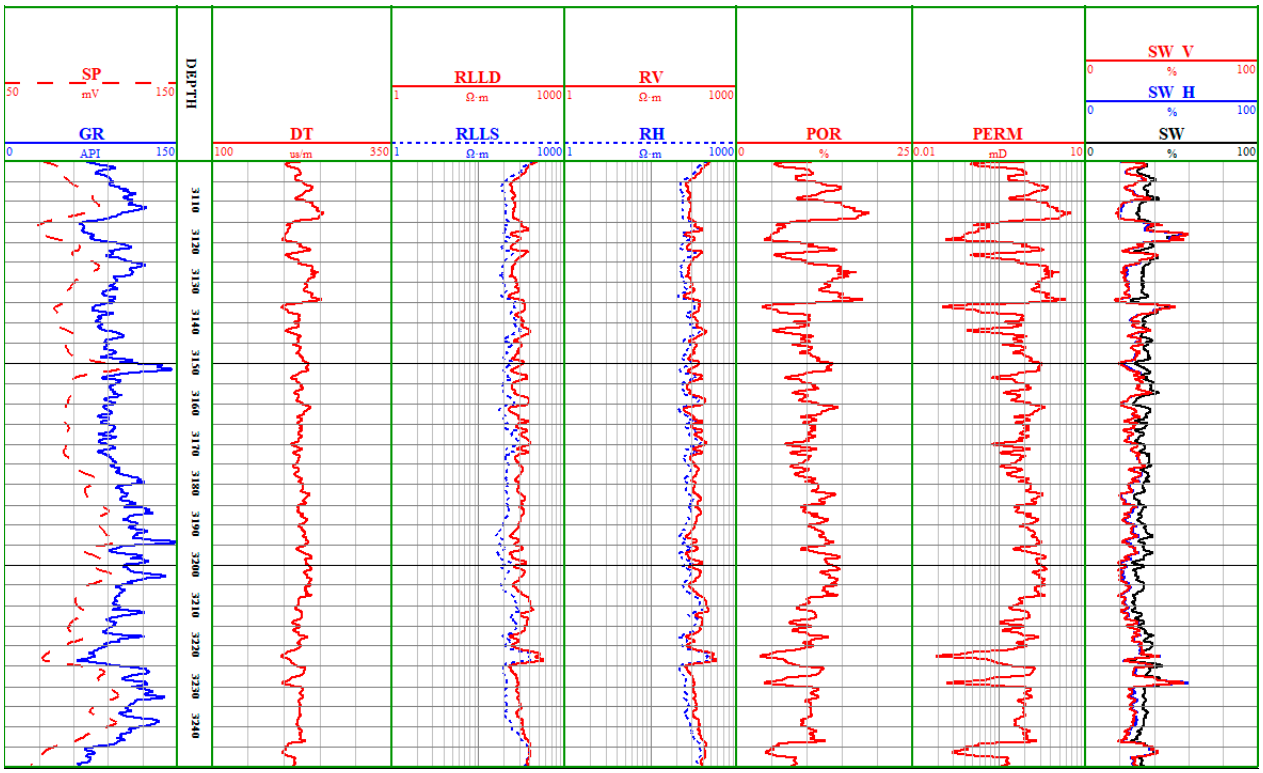

Figure 19. Comparisons of calculated water saturations by using apparent deep lateral resistivity, corrected horizontal and vertical resistivities separately.

4.3. Formation Classification Based on Pore Structure

The ultimate purpose of formation evaluation is to determine the highest-quality intervals, and offer the optimal development zones. Hence, establishing formation classification criteria is indispensable. Generally, formation quality is heavily controlled by pore structure, oil volume, and permeability, and they significantly affect the movable fluid saturation. The greater the change in permeability, the more significant the change in movable fluid saturation. Pore structure is the main factor that contributes to the obviously different occurrence characteristics of movable fluid [41]. Formation pore structure can be characterized by the shape of the pore-throat radius. Generally, rocks with good pore structure always contain wide pore-throat radius distribution, and it exhibits bimodality or multimodality. However, narrow unimodal pore-throat radius always corresponds to relatively simple pore structure. Hence, many parameters that are extracted from pore-throat radius distributions, e.g., the average pore-throat radius (R_m), R_{max}, the median pore-throat radius ($R50$), are used to represent the pore structure. In the Chang 8 Formation of Shunning Region, the pore-throat radius distributions are acquired from MICP experimental data of 20 core samples in the vertical direction, and the relationship between formation quality and pore-throat radius distribution is compared. Figure 20a,c,e display the pore-throat radius spectra of three typical core samples of No.1, No.5, and No.13, and Figure 20b,d,f display the experimented NMR T_2 distributions of these three core samples. Comparisons clearly illustrate that the pore-throat radius distribution match well with NMR. Hence, the pore-throat radius distributions can replace NMR T_2 spectra to characterize formation pore structure once the NMR data had not been consecutively acquired.

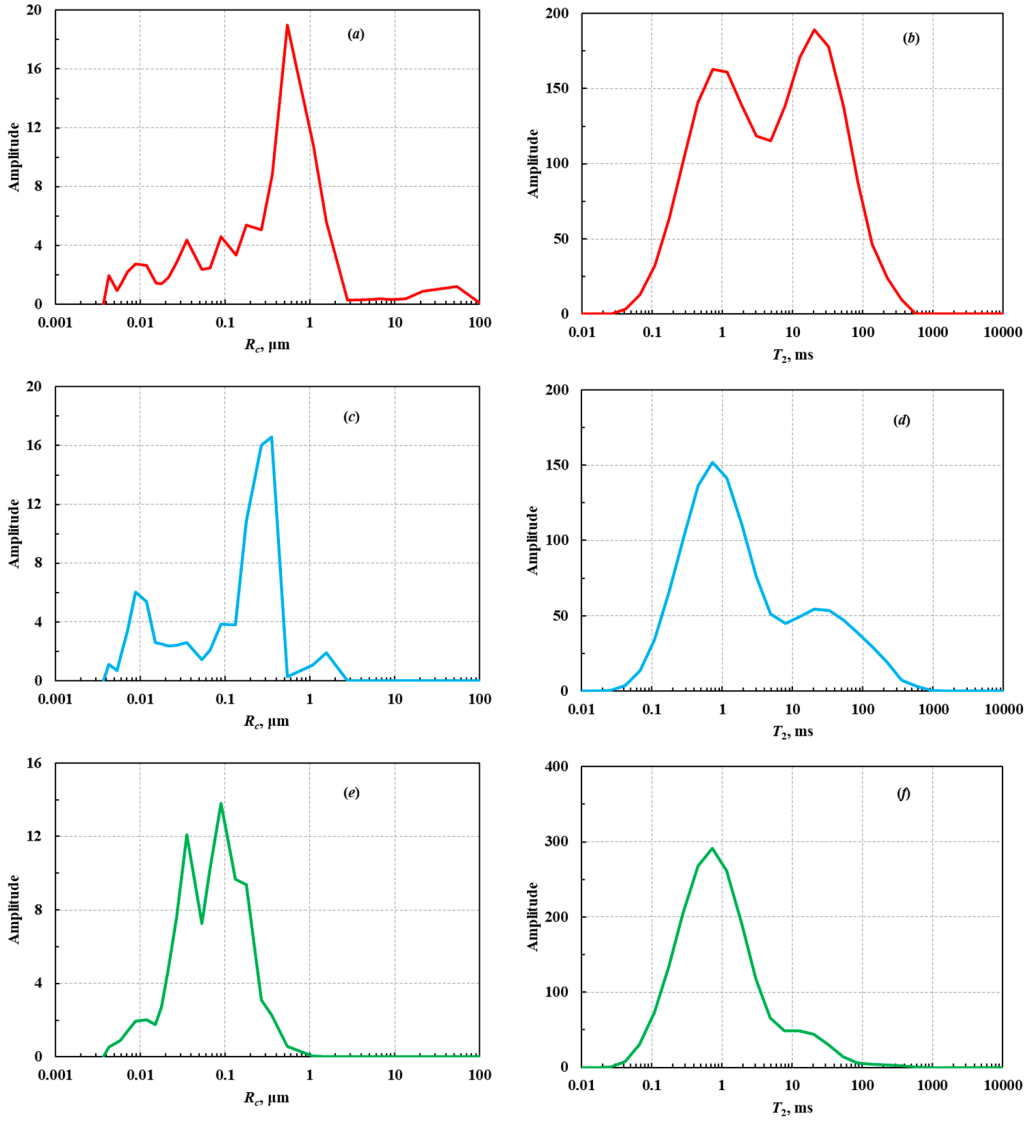

Figure 20. Comparison of pore-throat radius spectra and the corresponding NMR T_2 distributions of rocks with good pore structure (**a**,**b**), medium pore structure (**c**,**d**) and simple pore structure (**e**,**f**) in Chang 8 Formation of Shunning Region.

Li et al. (2023) pointed out that the pore-throat radius distribution can be reconstructed from conventional well logs based on the deep-learning method [42]. This method has been verified to be widely usable in the Ordos Basin [43]. Hence, the raised method by Li et al. (2023) is directly used in our target Chang 8 Formation in the horizontal well. The pore-throat radius distributions are consecutively constructed. Afterward, R_m is consecutively calculated to reflect formation pore structure characteristic.

In addition, hydrocarbon volume is also an important parameter that controls formation quality. Generally, high-quality reservoirs always contain high hydrocarbon volume and, thus, good production. On the contrary, once the hydrocarbon volume is low, the corresponding reservoir quality is also poor [44]. Hence, hydrocarbon (oil in the Chang 8 Formation) volume is also considered as an input parameter in establishing formation classification criteria in the horizontal well. Based on the definition, oil volume is calculated as:

$$f_o = \varphi \times S_o = \varphi \times (1 - S_w) \quad (16)$$

where f_o is the oil volume in %; S_o is the oil saturation in v/v.

Based on the above analysis, we chose two parameters of R_m and f_o, which respectively reflect the pore structure and formation quality to establish the formation type indicator parameter. This parameter is calculated as follows:

$$FTI = R_m \times f_o = R_m \times \varphi \times (1 - S_w) \quad (17)$$

where *FTI* is the formation type indicator parameter in the horizontal well.

By using Equation (17), we process the Chang 8 Formation in 17 horizontal wells, which contain drill stem test (DST) data, in our target region, and *FTI*s are calculated. Relationships among *FTI* and formation physical property parameters (porosity, permeability, and *DT*) are analyzed. Finally, we establish formation classification criteria (Figure 21). Based on the criteria, our target Chang 8 Formation is classified into four types. The classification criteria are listed in Table 1. The first type of formation contains the best pore structure, the highest f_o, and, thus, the highest-quality and oil production. The pore structure and f_o of the second type of formation are relatively weaker than that of the first type of formation, and the quality is also poorer. The third type of formation is poorer oil-bearing formation due to lower *FTI* and physical property parameter. The last type of formation is the dry layer; no development program should be made for this type of formation.

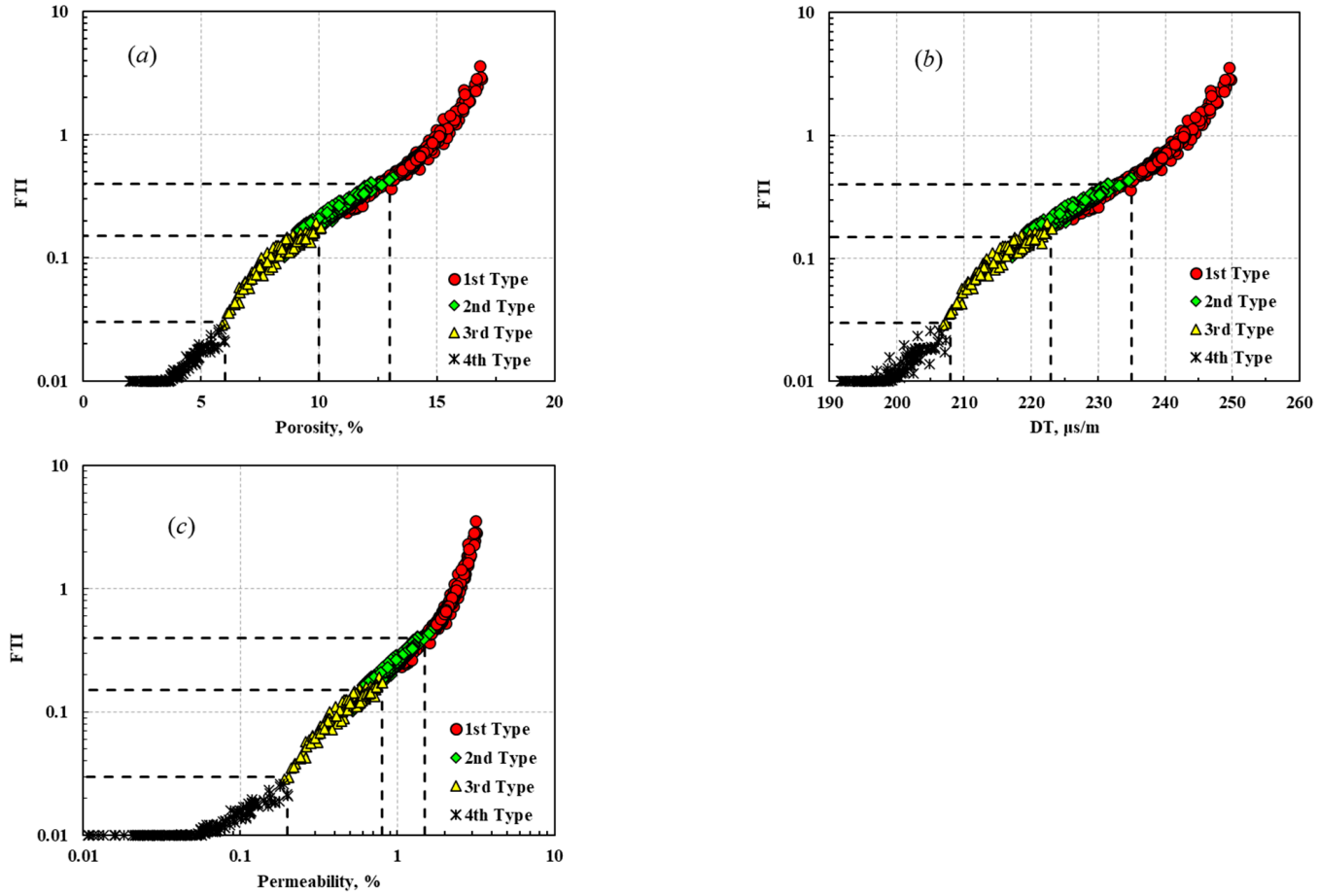

Figure 21. Cross-plots of formation type indicator parameter with porosity (**a**), interval transit time (**b**) and permeability (**c**) respectively. Based on this, horizontal well classification criteria in Chang 8 Formation of Shunning Region was established.

Table 1. Formation classification criteria in horizontal wells of Shunning Region, Central Ordos Basin.

Reservoir Type	Interpretation Result	*FTI*	f_o	V_{sh} (%)	Formation Physical Property Parameter		
					AC (μs/m)	Porosity (%)	Permeability (mD)
1st type	The highest-quality oil-bearing formation	≥0.4	≥6.5	15.0~20.0	≥235.0	≥13.0	≥1.5
2nd type	Relative high-quality oil-bearing formation	0.15~0.4	3.5~6.5	18.0~25.0	223.0~235.0	10.0~13.0	0.8~1.5
3rd type	Poorer oil-bearing formation	0.03~0.15	1.0~3.5	19.0~27.0	208.0~223.0	6.0~10.0	0.2~0.8
4th type	Dry layer	<0.03	<1.0	15.0~25.0	<208.0	<6.0	<0.2

5. Case Studies

The proposed models and formation classification criteria are applied to our target Chang 8 Formation in two horizontal wells B and C. After the anisotropy of DT and RT are corrected, formation porosity, water saturation, and oil volume are calculated. Afterwards, *FTI* is calculated to classify horizontal intervals and determine the highest-quality "sweet spot" area. Figures 22 and 23 display the formation classification results based on the criteria that are listed in Table 1. The evaluation results illustrate that the first and second types of formations are dominant in the horizontal interval in Well B; the total amount reaches to 76.4%. Especially for the first type of formation, it contributes the most to oil production capacity. The fourth type of formation can be ignored. This means that the reservoir quality is greater. However, in the horizontal interval in Well C, the proportion of the first type reservoir is only 3.4%, but the amount of the third reservoir reaches to 52.6%.

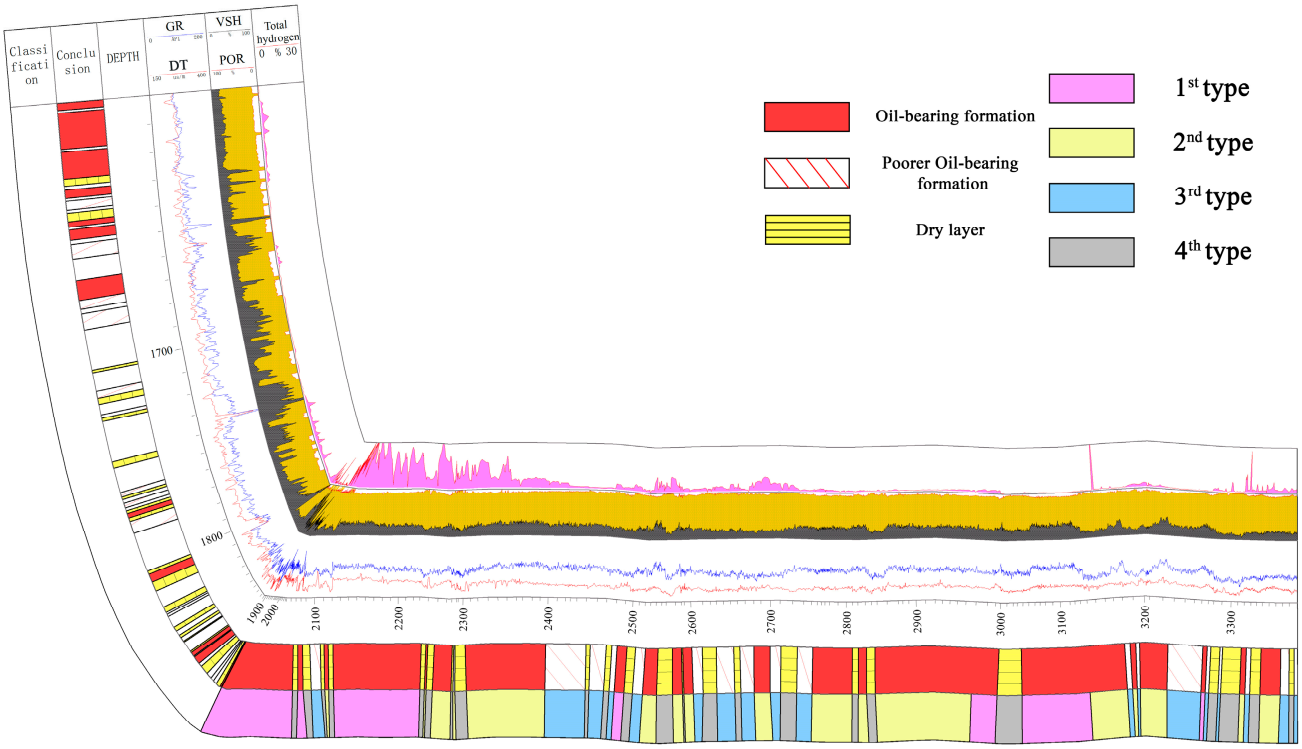

Figure 22. A field example of evaluating and classifying horizontal interval in Well B based on our raised methods and techniques.

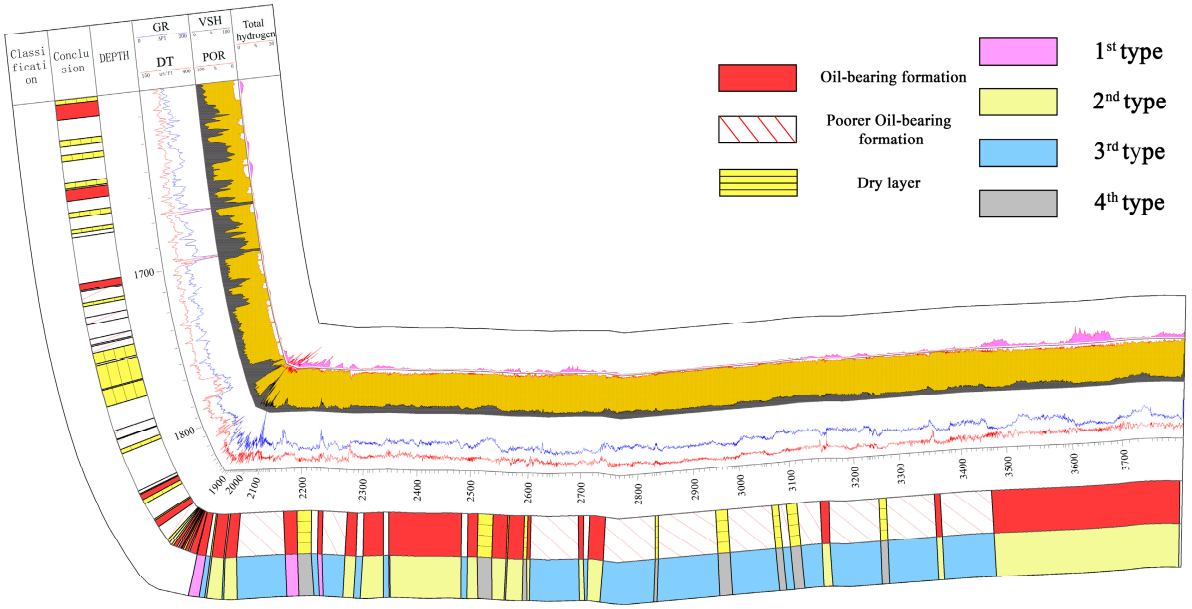

Figure 23. A field example of evaluating and classifying horizontal interval in Well C based on our raised methods and techniques.

Comparison of formation classification in these two wells illustrates that Well B has great0er reservoir quality despite the longer horizontal interval of Well C. Hence, we predict that Well B will contain much more oil production capacity. This prediction is verified by the drill stem test data. In Well B, approximately 74.16 bbl of oil is produced per day. However, in Chang 8 Formation of Well C, only 26.28 bbl of oil is produced per day; the daily oil production of Well C is only one-third as much as that of Well B.

To quantize the relationship between formation quality and oil production, we extract the total proportion of first and second types of formation (these two types of formation have a dominant contribution to oil production capacity in Chang 8 Formation) and find that it is heavily positively associated with daily oil production (Figure 24). With the increase of the total proportion of the first and second types of formation, daily oil production per meter increases.

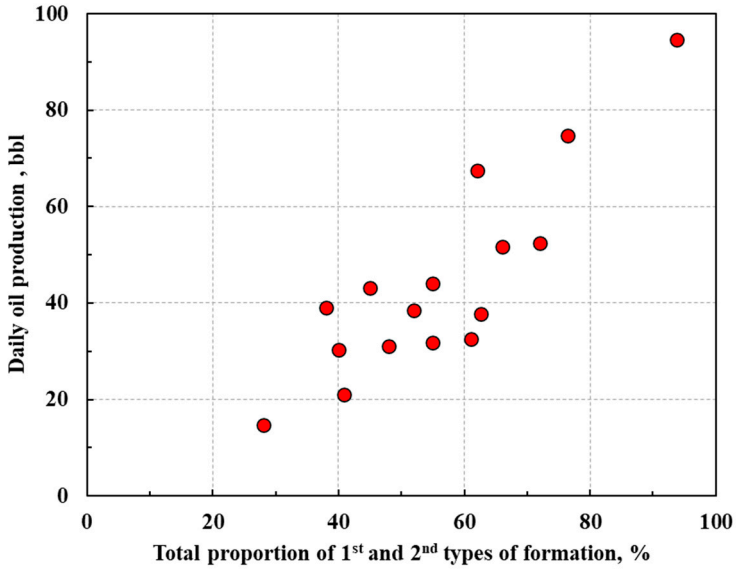

Figure 24. Cross-plot of the total proportion of 1st and 2nd types of formation versus daily oil production. Positive relationship means the dominant contribution of formation quality to oil production capacity, especially the high-quality formation.

6. Discussions

In this study, we raise methods and models of correcting the anisotropy of interval transit time and deep lateral resistivity, calculating formation parameter and classifying formation type in horizontal wells, and well results are acquired in our target Chang Formation in Shunning Region, Central Ordos Basin. However, these methods and models are all established based on experimented results of typical core samples and drill stem test data. This means they are only valuable in the Chang 8 Formation. In other regions, these methods and models, especially the formation classification criteria, may not be available unless they contain similar formation properties. If we want to apply the established methods and models in any other formation, a certain amount of core samples should be first drilled for petrophysical experiments to calibrate the involved parameters in our raised models. In addition, the corresponding drill stem test data should also be acquired to adjust the established criteria in Table 1.

7. Conclusions

The Triassic Chang 8 Formation in Shunning Region belongs to typical tight sandstone reservoirs, and the heterogeneity of interval travel time, resistivity, and pore structure are strong. It is difficult to accurately calculate formation physical property parameters and characterize the pore structure in horizontal wells before the anisotropy of interval travel time and resistivity is first corrected.

After the anisotropy of apparent resistivity of the horizontal well is corrected, two resistivities, the horizontal and vertical resistivities, are acquired. The Archie's equation is respectively optimized, and the water saturations in horizontal and vertical directions are calculated. Consistency of these two water saturations verifies the reliability of resistivity anisotropy correction. Meanwhile, interval travel time anisotropy is also corrected to predict formation porosity in horizontal intervals.

Relationships among hydrocarbon volume, pore structure, and formation quality are analyzed, and we raise an assembly parameter of *FTI* to identify high-quality formation in Chang 8 Member. Combined with *FTI* and drill stem test data, our target horizontal intervals of Chang 8 Formation are classified into four types. The first type of formation contains the highest quality, and it has the greatest contribution to oil production capacity. The pore structure and *FTI* of second and third types of formation are poorer than that of the first type of formation, the formation quality and production capacity are also poorer. The fourth type of formation is dry layer; no hydrocarbon can be produced.

The total proportion of first and second types of formation is positively associated with daily oil production. Hence, once the pore structure is first characterized, the proportion of four types of formation can be identified. Afterward, the total proportion of first and second types of formation can be calculated to predict oil production capacity in our target horizontal intervals in Chang 8 Formation of the Shunning Region.

Author Contributions: Software, R.C. and H.W.; Formal analysis, H.X.; Investigation, W.Z.; Writing—original draft, J.L.; Writing—review & editing, L.X.; Supervision, L.X. All authors have read and agreed to the published version of the manuscript.

Funding: This research was supported by the National Natural Science Foundation of China (No. 41302106), the China Postdoctoral Science Foundation (No. 2012M520347, 2013T60147), the Fundamental Research Funds for the Central Universities, China (No. 2-9-2016-007), and the MOST Special Fund from the State Key Laboratory of Geological Processes and Mineral Resources, China University of Geosciences.

Data Availability Statement: The data presented in this study are available on request from the corresponding author. The data are not publicly available due to restrictions of privacy.

Conflicts of Interest: The authors declare no conflict of interest.

References

1. Clavier, C. The challenge of logging horizontal wells. *Log Anal.* **1991**, *32*, 63–84.
2. Liu, X.; Yang, X.; He, X.; Wu, J.; Meng, Q. Relationship between horizontal well trajectory and formation analysis in Longdong tight oil area. *J. S. Pet. Univ. (Sci. Technol. Ed.)* **2017**, *39*, 51–60.
3. Zhang, P. Research on Horizontal Well Formation Evaluation Method Based on Acoustic and Resistivity Logging. Master's Dissertation, China University of Petroleum, Qingdao, China, 2016; pp. 1–4.
4. Zhou, C.; Wang, C. Technology review on the log interpretation of horizontal well. *Prog. Geophys.* **2006**, *21*, 152–160.
5. Ren, L.; Su, Y.; Wang, W.; Zhao, G.; Yuan, B. Seepage characteristics and productivity distribution of segmented multi-cluster fractured horizontal wells. *J. Xi'an Shiyou Univ. (Nat. Sci. Ed.)* **2013**, *28*, 55–59.
6. Moran, J.H.; Gianzero, S. Effects of formation anisotropy on resistivity-logging measurements. *Geophysics* **1979**, *44*, 1266–1286. [CrossRef]
7. Klein, J. Induction log anisotropy corrections. *Log Anal.* **1993**, *34*, 18–27.
8. Gao, J.; Xie, R. 3D numerical forward modeling and fast correction of dual-laterolog for high angle deviated wells. *Pet. Explor. Dev.* **2000**, *27*, 69–71.
9. Sun, J.; Zhang, P.; Feng, C.; Liu, X. Research on Horizontal Well Formation Evaluation in LS Oilfield. *Well Logging Technol.* **2016**, *40*, 675–682.
10. Liu, X.; Cao, M.; Jing, H.; Zhang, W.; Zhang, P.; Wang, G.; Li, Y.; Xie, L. Correction of acoustic time anisotropy of horizontal wells in Longdong area, Ordos Basin. *China Pet. Explor.* **2022**, *27*, 143–148.
11. He, D.; Jia, A.; Ji, G.; Wei, Y.; Tang, H. Well type and pattern optimization technology for large scale tight sand gas, Sulige gas field, NW China. *Pet. Explor. Dev.* **2013**, *40*, 84–95. [CrossRef]
12. Wei, Y.; Jia, A.; He, D.; Liu, Y.; Ji, G.; Cui, B.; Ren, L. Classification and evaluation of horizontal well performance in Sulige tight gas reservoirs, Ordos Basin. *Nat. Gas Ind.* **2013**, *33*, 47–51.
13. Li, T.; Huang, X. Classification of horizontal wells based on dynamic data and its application in ultra-low permeability gas reservoirs. *Chem. Technol. Fuels Oils* **2017**, *53*, 123–134. [CrossRef]
14. Lu, S.; Li, J.; Zhang, P.; Xue, H.; Wang, G.; Zhang, J.; Liu, H.; Li, Z. Classification of microscopic pore-throats and the grading evaluation on shale oil reservoirs. *Pet. Explor. Dev.* **2018**, *45*, 452–460. [CrossRef]
15. Wang, B.; Liu, X.; SIMA, L. Grading evaluation and prediction of fracture-cavity reservoirs in Cambrian Longwangmiao Formation of Moxi area, Sichuan Basin, SW China. *Pet. Explor. Dev.* **2019**, *46*, 301–313. [CrossRef]
16. Zhang, M. Quantitative evaluation method of gas content for shale gas horizontal well: A case study of Fuling shale gas field, Sichuan Basin. *Mar. Orig. Pet. Geol.* **2019**, *24*, 78–84.
17. Luan, B.; Zhang, B.; Wang, D.; Deng, C.; Wang, F. Quantitative evaluation of tight oil reservoirs in the Chang 8 Member of the Yanchang Formation in southern Ordos Basin. *Front. Earth Sci.* **2022**, *10*, 963316. [CrossRef]
18. Wang, J.; Wu, S.; Li, Q.; Zhang, J.; Guo, Q. Characterization of the pore-throat size of tight oil reservoirs and its control on reservoir physical properties: A case study of the Triassic tight sandstone of the sediment gravity flow in the Ordos Basin, China. *J. Pet. Sci. Eng.* **2020**, *186*, 106701. [CrossRef]
19. Deng, J.; Wang, Q.F.; Gao, B.F.; Huang, D.H.; Yang, L.Q.; Xu, H.; Zhou, Y.H. Evolution of Ordos Basin and Its Distribution of Various Energy Resources. *Geoscience* **2005**, *19*, 538–545.
20. Zhao, Z.; Liu, C. *The Forming and Evolution of North China Craton Depositional Basin and Hydrocarbon Accumulation*; Northwest University Press: Xi'an, China, 1990; pp. 1–189.
21. Wu, B.; Zhang, W.; Song, Z.; Cun, X.; Sun, L.; Luo, J.; Li, Y.; Cheng, X.; Sun, B. Geological and Geochemical Characteristics of Uranium Minerals in the Sandstone-type Uranium Deposites in the North of Ordos Basin and Their Genetic Significance. *Acta Geol. Sin.* **2016**, *90*, 3393–3407.
22. Yang, B. Sedimentary Facies of Chang 9 Oil Formation of the Yanchang Formation in Zhijing-Ansai Area, Ordos Basin. Master Dissertation, Northwest University, Xi'an, China, 2014; pp. 7–10.
23. Wang, X.; Liu, N.; Nan, J.; Wang, X.; Ren, D. Characteristics and Genetic Mechanism of Chang Eight Low Permeability and Tight Reservoir of Triassic Yanchang Formation in Central-East Ordos Basin. *Front. Phys.* **2022**, *9*, 801264. [CrossRef]
24. Li, X.; Liu, X.; Zhou, S.; Liu, H.; Chen, Q.; Wang, J.; Liao, J.; Huang, J. Hydrocarbon origin and reservoir forming model of the Lower Yanchang Formation, Ordos Basin. *Pet. Explor. Dev.* **2012**, *39*, 184–193. [CrossRef]
25. Liu, H.; Zhao, Y.; Luo, Y.; Xiao, G.; Meng, Y.; Zhou, S.; Shao, L. Origin of the reservoir quality difference between Chang 8 and Chang 9 Member sandstones in the Honghe Oil Field of the Southern Ordos Basin, China. *J. Pet. Sci. Eng.* **2020**, *185*, 106668. [CrossRef]
26. Coates, G.R.; Xiao, L.; Primmer, M.G. *NMR Logging Principles and Applications*; Gulf Publishing Company: Houston, TX, USA, 2000; pp. 1–256.
27. Xiao, L.; Mao, Z.; Li, G.; Jin, Y. Estimation of saturation exponent from nuclear magnetic resonance (NMR) logs in low permeability reservoirs. *Appl. Magn. Reson.* **2013**, *44*, 333–347. [CrossRef]
28. Xiao, L.; Zou, C.; Mao, Z.; Shi, Y.; Liu, X.; Jin, Y.; Guo, H.; Hu, X. Estimation of water saturation from nuclear magnetic resonance (NMR) and conventional logs in low permeability sandstone reservoirs. *J. Pet. Sci. Eng.* **2013**, *108*, 40–51. [CrossRef]
29. Raymer, L.; Hunt, E.; Gardner, J. An improved sonic transit time-to-porosity transform. In Proceedings of the SPWLA 21st Annual Logging Symposium, Lafayette, Louisiana, 8–11 July 1980.

30. Xiao, L.; Liu, X.; Zou, C.; Hu, X.; Mao, Z.; Shi, Y.; Guo, H.; Li, G. Comparative study of models for predicting permeability from nuclear magnetic resonance (NMR) logs in two Chinese tight sandstone reservoirs. *Acta Geophys.* **2014**, *62*, 116–141. [CrossRef]
31. Swanson, B.F. A simple correlation between permeabilities and mercury capillary pressures. *J. Pet. Technol.* **1981**, *33*, 2498–2504. [CrossRef]
32. Zhang, H.; Li, G.; Guo, H.; Zhang, W.; Wang, Y.; Li, W.; Zhou, J.; Wang, C. Applications of nuclear magnetic resonance (NMR) logging in tight sandstone reservoir pore structure characterization. *Arab. J. Geosci.* **2020**, *13*, 572. [CrossRef]
33. Archie, G.E. The electrical resistivity log as an aid in determining some reservoir characteristics. *Trans. AIME* **1942**, *146*, 54–62. [CrossRef]
34. Simandoux, P. Dielectric measurements on porous media, application to the measurements of water saturation: Study of behavior of argillaceous formations. *Rev. L'institut Fr. Pet.* **1963**, *18*, 193–215.
35. Leveaux, J.; Poupon, A. Evaluation of water saturation in shaly formations. In Proceedings of the SPWLA 12th Annual Logging Symposium, Dallas, TX, USA, 2–5 May 1971.
36. Waxman, M.H.; Smits, L.J.M. Electrical conductivities in oil-bearing shaly sands. *Soc. Pet. Eng. J.* **1968**, *8*, 107–122. [CrossRef]
37. Waxman, M.H.; Thomas, E.C. Electrical conductivities in shaly sands-I. The relation between hydrocarbon saturation and resistivity index; II. The temperature coefficient of electrical conductivity. *J. Pet. Technol.* **1974**, *26*, 213–225. [CrossRef]
38. Clavier, C.; Coates, G.; Dumanoir, J. Theoretical and experimental bases for the dual-water model for interpretation of shaly sands. *Soc. Pet. Eng. J.* **1984**, *24*, 153–168. [CrossRef]
39. Givens, W.W. A conductive rock matrix model (CRMM) for the analysis of low-contrast resistivity formations. *Log Anal.* **1987**, *28*, 138–151.
40. Gao, F.; Xiao, L.; Zhang, W.; Cui, W.; Zhang, Z.; Yang, E. Low Permeability Gas-Bearing Sandstone Reservoirs Characterization from Geophysical Well Logging Data: A Case Study of Pinghu Formation in KQT Region, East China Sea. *Processes* **2023**, *11*, 1030. [CrossRef]
41. Li, P.; Sun, W.; Wu, B.; Huang, R.; Gao, Y.; Yan, J.; Huang, H. Occurrence characteristics and main controlling factors of movable fluids in Chang 81 reservoir, Maling Oilfield, Ordos Basin, China. *J. Petrol. Explor. Prod. Technol.* **2019**, *9*, 17–29. [CrossRef]
42. Li, G.; Zhang, W.; Liu, D.; Li, J.; Li, J.; Xiao, L. Characterization of Tight Sandstone Reservoir Pore Structure and Validity from Geophysical Logging Data by Using Deep Learning Method. In Proceedings of the SPE Gas & Oil Technology Showcase and Conference, Dubai, United Arab Emirates, 13 March 2023. [CrossRef]
43. Li, F.; Zhang, W.; Li, W.; Chen, Z.; Sun, B.; Chi, R.; Li, G.; Xiao, L. Tight Sandstone Reservoir Pore Structure Characterization from Conventional Well Logging Data Based on Machine Learning Method. In Proceedings of the SPWLA 27th Formation Evaluation Symposium of Japan, Virtual, 16 September 2022.
44. Sun, N. Study on Sedimentary Characteristics and Reservoir Desification Mechanism of Sediment Gravity Flow of Yanchang Formation in Southern Ordos Basin, China. Ph.D. Dissertation, China University of Petroleum, Qingdao, China, 2019; pp. 1–3.